circPVT1 and PVT1/AKT3 show a role in cell proliferation, apoptosis, and tumor subtype-definition in small cell lung cancer

Tolomeo, Doron; Traversa, Debora; Venuto, Santina; Ebbesen, Karoline K.; García Rodríguez, Juan L.; Tamma, Grazia; Ranieri, Marianna; Simonetti, Giorgia; Ghetti, Martina; Paganelli, Matteo

Published in:
Genes Chromosomes and Cancer

DOI:
10.1002/gcc.23121

Received: 7 October 2022 | Revised: 6 December 2022 | Accepted: 12 December 2022

DOI: 10.1002/gcc.23121

WILEY

RESEARCH ARTICLE

circPVT1 and *PVT1/AKT3* show a role in cell proliferation, apoptosis, and tumor subtype-definition in small cell lung cancer

Doron Tolomeo[1] | Debora Traversa[1] | Santina Venuto[2] | Karoline K. Ebbesen[3] | Juan L. García Rodríguez[4] | Grazia Tamma[1] | Marianna Ranieri[1] | Giorgia Simonetti[5] | Martina Ghetti[5] | Matteo Paganelli[5] | Grazia Visci[1] | Arcangelo Liso[2] | Klaas Kok[6] | Lucia Anna Muscarella[7] | Federico Pio Fabrizio[7] | Maria Antonia Frassanito[8] | Aurelia Lamanuzzi[8] | Ilaria Saltarella[8] | Antonio Giovanni Solimando[8] | Alessandro Fatica[9] | Zaira Ianniello[9] | René Massimiliano Marsano[1] | Antonio Palazzo[1] | Amalia Azzariti[10] | Vito Longo[11] | Stefania Tommasi[12] | Domenico Galetta[11] | Annamaria Catino[11] | Alfredo Zito[13] | Tommaso Mazza[14] | Alessandro Napoli[14] | Giovanni Martinelli[5] | Jørgen Kjems[3] | Lasse Sommer Kristensen[4] | Angelo Vacca[8] | Clelia Tiziana Storlazzi[1]

[1]Department of Biosciences, Biotechnology and Environment, University of Bari Aldo Moro, Bari, Italy

[2]Department of Medical and Surgical Sciences, University of Foggia, Foggia, Italy

[3]Interdisciplinary Nanoscience Centre (iNANO), Aarhus University, Aarhus, Denmark

[4]Department of Biomedicine, Aarhus University, Aarhus, Denmark

[5]Biosciences Laboratory, IRCCS Istituto Romagnolo per lo Studio dei Tumori (IRST) "Dino Amadori", Meldola (FC), Italy

[6]Department of Genetics, University of Groningen, University Medical Center Groningen, Groningen, The Netherlands

[7]Laboratory of Oncology, Fondazione IRCCS "Casa Sollievo della Sofferenza", San Giovanni Rotondo (FG), Italy

[8]Department of Precision and Regenerative Medicine and Ionian Area - (DiMePRe-J), School of Medicine, Aldo Moro University of Bari, Bari, Italy

[9]Department of Biology and Biotechnology "Charles Darwin", Sapienza University of Rome, Rome, Italy

[10]Laboratory of Experimental Pharmacology, IRCCS Istituto Tumori Giovanni Paolo II, Bari, Italy

[11]Medical Thoracic Oncology Unit, IRCCS Istituto Tumori Giovanni Paolo II, Bari, Italy

[12]Molecular Diagnostics and Pharmacogenetics Unit, IRCCS Istituto Tumori Giovanni Paolo II, Bari, Italy

[13]Pathology Unit, IRCCS Istituto Tumori Giovanni Paolo II, Bari, Italy

[14]Bioinformatics Unit, Fondazione IRCCS "Casa Sollievo della Sofferenza", San Giovanni Rotondo (FG), Italy

Correspondence
Clelia Tiziana Storlazzi, Department of Biosciences, Biotechnology and Environment, University of Bari Aldo Moro, Via E. Orabona no.4, 70125 Bari, Italy.
Email: cleliatiziana.storlazzi@uniba.it

Abstract

Small cell lung cancer (SCLC) is treated as a homogeneous disease, although the expression of NEUROD1, ASCL1, POU2F3, and YAP1 identifies distinct molecular subtypes. The *MYC* oncogene, amplified in SCLC, was recently shown to act as a lineage-specific factor to associate subtypes with histological classes. Indeed,

Doron Tolomeo and Debora Traversa contributed equally to this work.

Present address
Debora Traversa, Molecular Diagnostics and Pharmacogenetics Unit, IRCCS Istituto Tumori Giovanni Paolo II, Bari, Italy.

Grazia Visci, Istituto di Biomembrane, Bioenergetica e Biotecnologie Molecolari (IBIOM), Consiglio Nazionale delle Ricerche, Bari, Italy.

Funding information
Associazione Italiana per la Ricerca sul Cancro, Grant/Award Number: 25706; Programma Operativo Nazionale Attrazione e Mobilità Internazionale, Grant/Award Number: 1807508-2

MYC-driven SCLCs show a distinct metabolic profile and drug sensitivity. To disentangle their molecular features, we focused on the co-amplified *PVT1*, frequently overexpressed and originating circular (circRNA) and chimeric RNAs. We analyzed hsa_circ_0001821 (circPVT1) and *PVT1/AKT3* (chimPVT1) as examples of such transcripts, respectively, to unveil their tumorigenic contribution to SCLC. In detail, circPVT1 activated a pro-proliferative and anti-apoptotic program when overexpressed in lung cells, and knockdown of chimPVT1 induced a decrease in cell growth and an increase of apoptosis in SCLC in vitro. Moreover, the investigated *PVT1* transcripts underlined a functional connection between MYC and YAP1/POU2F3, suggesting that they contribute to the transcriptional landscape associated with *MYC* amplification. In conclusion, we have uncovered a functional role of circular and chimeric *PVT1* transcripts in SCLC; these entities may prove useful as novel biomarkers in *MYC*-amplified tumors.

KEYWORDS
circular RNA, fusion transcript, MYC, PVT1, small cell lung cancer

1 | INTRODUCTION

Small cell lung cancer (SCLC) is the most devastating type of lung cancer, accounting for 15% of all cases[1] and a 5-year survival rate of 1%–5%. Therapies have remained unchanged in the last 40 years, consisting of chemotherapy regimens at all disease stages. In the last few years, immunotherapy based on atezolizumab and durvalumab, used in combination with platinum-based chemotherapy, was approved in extensive-stage SCLC.[2] However, these therapies showed a modest effect in patients' overall survival (12.3 vs. 10.3 months, HR 0.70, $p = 0.007$; 13 vs. 10.03 months, HR 0.73, $p = 0.0047$, respectively[3–5]). Recently, similar results have been reported in two Asiatic trials, confirming only a modest advantage of immunotherapy added to chemotherapy.[6,7] Moreover, cost-effectiveness analysis is not favorable for chemoimmunotherapy in SCLC patients.[8] Surgical removal is generally restricted to a few cases; thus, in-depth molecular studies of large cohorts are limited.[9] In 2019, four SCLC subtypes were defined through the differential expression of lineage-specific transcription factors: ASCL1 (SCLC-A subtype), NEUROD1 (SCLC-N subtype), POU2F3 (SCLC-P subtype), and YAP1 (SCLC-Y subtype),[10,11] raising opportunities for personalized treatments. More recently, Gay et al. identified a high YAP1 expression in other subtypes, pointing out that this molecule may not indicate a specific SCLC subtype.[12] These authors suggest a T-cell inflamed or SCLC-I subtype, with a high expression of immune-related genes, as the fourth patient subtype, in addition to SCLC-A/N/P.[13] Notably, each subtype displays a specific therapeutic vulnerability,[4,5,14–16] suggesting that distinct molecular features could be at the basis of this classification.[10] Moreover, the *MYCL* and *MYC* paralogs (showing a mutually exclusive high-copy number gain in 9% and 6% of SCLC, respectively[17]) were recently described as lineage-specific factors to associate SCLC molecular subtypes with histological classes. In detail, *MYCL* and *MYC* were shown to impart neuronal and non-neuroendocrine–associated transcriptional programs.[17,18] Enforced expression of *MYC* is observed to drive a subtype shifting from SCLC-A to SCLC-N to SCLC-Y.[18] Indeed, *MYC* over-expression is incompatible with the SCLC-A subtype, as *MYC*-high SCLC subtypes correspond to ASCL1-low samples.[17] Worthy, *MYC*-overexpressing SCLCs exhibited an increased vulnerability to indirect MYC inhibitors, such as Aurora A/B kinase and CHK1-inhibitors, compared with *MYCL*- or *MYCN*-overexpressing tumors.[15,19] Furthermore, BET and PARP-1 inhibitors showed a synergistic effect on suppressing the growth and survival of SCLC cells carrying *MYC* amplification over non-tumor cells.[20]

This evidence underlines the need to disentangle the molecular bases behind the SCLC subtype definition to identify novel and specific biomarkers for better patient stratification and personalized therapies.[19] Interestingly, we and others previously showed that SCLC cell lines and primary tumors with *MYC* amplification overexpress the co-amplified *Plasmacytoma Variant Translocation 1* (*PVT1*) gene (8q24.21).[21,22] This gene belongs to the class of long non-coding RNAs (lncRNAs), that is, RNA entities of more than 200 nt in size with a low protein-coding potential. High transcriptional plasticity characterizes *PVT1*; it gives rise to 176 linear and 29 circular splicing variants, according to the Ensembl Genome Browser v107 (https://www.ensembl.org/index.html) and the CircInteractome database (https://circinteractome.nia.nih.gov/) respectively, of which the PVT1-224 linear and the hsa_circ_0001821 isoforms (herein referred to as PVT1 and circPVT1) are the best characterized at the molecular and functional level. These two transcripts share the sequence of the *PVT1* (NR_003367.3) exon 2, and increasing literature documents their role in promoting cell growth and invasion in non-small cell lung cancer (NSCLC)[23–33] and other tumor types,[34] where they represent potential novel diagnostic/prognostic biomarkers.

Moreover, *PVT1* is recurrently involved in the genesis of chimeras in hematological and solid tumors, including SCLC.[35,36] Chimeras are

powerful driver alterations clarly associated with peculiar tumor subtypes in lung cancer.[37,38]

Despite its role in tumor initiation and progression, also through the interaction with MYC,[39] only one study analyzes the function of *PVT1* in SCLC, and it is limited to the linear isoform.[40] Therefore, this gene and its multiple transcripts deserve further investigation. To address the role of *PVT1* isoforms in SCLC carcinogenesis and tumor progression, we here focus on circPVT1 and the *PVT1/AKT3* chimera (chimPVT1), the latter originated by the juxtaposition of the *PVT1* exon 1 to *AKT3* exon 2 and coding a shorter form of the AKT3 protein,[22] as examples of *PVT1* circRNA and fusion entities, respectively.

Our in vitro functional studies demonstrated that *PVT1* transcripts elicit lung cell proliferation, reduce the apoptosis rate, and impact the expression of MYC, *BCL2*, and the YAP1 and POU2F3 master regulators. Furthermore, *PVT1* transcripts were detectable in the extracellular vesicles (EVs) secreted by SCLC cell lines, thus unveiling their potential as biomarkers for noninvasive liquid biopsy-based approaches. Overall, our observations uncover a vulnerability of this recalcitrant cancer and provide a rationale for *PVT1* therapeutic targeting, especially for the *MYC*-amplified SCLC subtypes.

2 | MATERIALS AND METHODS

2.1 | In silico analysis of *PVT1* expression in SCLC data sets

Seventeen control lung tissues and six small cell lung carcinomas were retrieved from the data set GSE83227 of the Gene Expression Omnibus database. The mRNA profiles of 12,600 transcripts of these samples were quantified using the Affymetrix Human Genome U95 Version 2 Array and analyzed with the *affy* and *limma* Bioconductor R packages. First, probeset signals were Robust Multichip Average (RMA) normalized. Then a linear model for each transcript was fitted, which was finally used to compute the differential expression between the two classes of samples by empirical Bayes moderation.

Transcriptomic data from seven normal lung tissues and 73 SCLC tissues were retrieved from the GSE60052 GEO data set. Sequenced short-reads were mapped onto release 41 of the GENCODE human reference transcriptome and counted using *STAR* version 2.6.1a_08-27.[41] STAR was run with standard parameters using the—quantMode GeneCounts mode. Differential expression analysis was performed with *DESeq2*,[42] which was run with standard parameters.

2.2 | Cell lines

Our study included five cell lines harboring *MYC* amplification (GLC1DM, GLC1HSR, GLC2, GLC3, NCI-H2171),[22,43,44] nine cell lines harboring *MYCL* (GLC26, GLC28, H1963, H510A, HCC33, H2141, H1184) or *MYCN* (GLC8, GLC14), but not *MYC* amplifications, used as controls. The BEAS-2B normal bronchial epithelial cell line and the HeLa cervix epithelioid carcinoma cell line were acquired from the American Type Culture Collection (ATCC, Manassas).

2.3 | RT-PCR assays

RT-PCR assays, Sanger sequencing, and RT-qPCR experiments were performed as described.[45,46]

Briefly, for RT-qPCR experiments, we tested 10 housekeeping genes (*ACTB*, *B2M*, *GAPDH*, *HMBS*, *HPRT1*, *RPL13A*, *SDHA*, *RNA28S*, *UBC*, and *YWHAZ*), choosing the best-performing ones (*GAPDH*, *SDHA*, and *HPRT1*) according to geNorm analysis,[47] and used them as normalization factors. The experiments were performed in triplicate. RT-qPCR results were analyzed by the REST[48] relative expression software tool (Table S1). Differential expression was considered significant with a p-value ≤0.05 at relative quantification. A commercial pooled normal lung RNA sample (Clontech, Diatech, Jesi, Italy; Cat. No. 636524) was also used as a calibrator in RT-qPCR assays. All primers are listed in Table S2.

2.4 | Cell transfection

We obtained a stably expressing circPVT1 cell line by transfecting BEAS-2B with an epB-Puro-TT derived plasmid harboring the *PVT1* exon 2 flanked by inverted repeats and expressing the Puromycin resistance gene (BEAS-2B$^{circPVT1/ND}$). All transfections were performed using the Lipofectamine 3000 Transfection Reagent (Thermo Fisher Scientific) according to the manufacturer's protocol. Positive cells were selected by antibiotic treatment (1 μg/ml), induced for circPVT1 expression by adding doxycycline hyclate (50 ng/ml), and evaluated at 24/48 h after induction with doxycycline (BEAS-2B$^{circPVT1/24D}$/BEAS-2B$^{circPVT1/48D}$). BEAS-2B^{eGFP} control cells were obtained by transfecting BEAS-2B with an epB-Puro-TT derived plasmid harboring the GFP gene.

To test the effect of MYC knockdown, this cell line was transfected with two specific small interfering RNAs (siRNAs) [siRNA1 *MYC* (VHS40785) and siRNA2 *MYC* (VHS40789), ThermoFisher Scientific, Rodano MI, Italy] specifically designed for *MYC* silencing by RNA interference. As a negative control, we used the si-NC 5′-AAUUCUCCGAACGUGUCACGU-3′ (Metabion), already used for this purpose.[49] 24 h after transfection, we evaluated the best-performing siRNA for *MYC* knockdown and chose siRNA2 *MYC*, showing a 65% expression reduction compared with the si-NC control.

A second model for circPVT1 overexpression was generated by cloning *PVT1* exon 2 into the pcDNA3.1 circRNA mini vector and transiently transfecting BEAS-2B cells. Functional studies were performed 24/48 h after the transfection (BEAS-2B$^{circPVT1/24tr}$/BEAS-2B$^{circPVT1/48tr}$). The same cells, transfected with the empty vector, were used as controls (BEAS-2B^{CTRL}).

Data obtained 24 h after circPVT1 Doxycycline induction/transient transfection were reported in the Tables S1 and S3.

To express the putative protein encoded by circPVT1, we engineered a transient expression vector (pcDNA3.1 3 × FLAG) harboring the longest circPVT1 ORF (104 aa) fused in frame with the FLAG tag and transfected it into HeLa cells (HeLa^{circPVT1}). A pcDNA3.1 3 × FLAG vector carrying the sequence of the circRNA circZNF609, whose coding activity has already been documented,[50] was used as a positive control (HeLa^{circZNF609}).

To test the biological function of chimPVT1, the GLC1HSR cell line was stably transfected with a piggyBac vector (VectorBuilder Inc.) encoding an shRNA that targeted the fusion junction (sh*PVT1/AKT3*: 5′-ATCTGCCCTCCAGAGAATATACTCGAGTATATTCTCTGGAGGGCAGAT-3′) (GLC1HSR^{shchimPVT1}). A scrambled shRNA (5′-CCTAAGG TTAAGTCGCCCTCGCTCGAGCGAGGGCGACTTAACCTTAGG-3′), targeting a nonspecific sequence, was used as a negative control (GLC1HSR^{Scram}). Both vectors carried a Puromycin resistance gene, allowing the selection of transfected cells (2 µg/ml of Puromycin).

All the functional analyses were carried out on three biological replicates.

2.5 | Northern blotting

Samples were pretreated with RNase R; 5 µg RNA was digested with one U RNase R (Lucigen) per µg in a total reaction volume of 10 µl for 10 min at 37°C. Control samples were treated similarly, but no RNase R was added to the reaction. After this, the samples were prepared for agarose Northern blotting by adding 20 µl of loading buffer. The samples were then heated at 65°C for 5 min, loaded onto a 1% agarose gel containing 3% formaldehyde and 1x MOPS, and run at 75 V in 1× MOPS for approximately 3 h after which RNA was transferred to a Hybond N^+ membrane (GE Healthcare) overnight. RNA was then UV cross-linked to the membrane and pre-hybridized in Church buffer (0.158 M NaH_2PO_4, 0.342 M Na_2HPO_4, 7% SDS, 1 mM EDTA, 0.5% BSA, pH 7.5) for 1 h. The membrane was probed with a 5′ radioactively labeled DNA oligonucleotide at 55°C (60-mer probe) overnight and washed twice in 2 × SSC, 0.1% SDS for 10 min at 45°C before exposure on a screen for data collection. The screen was developed on a Typhoon imager. The sequences of the used probes are the following: PVT1 exon 2 (CATCAGGCTCAGAAAATACTTGAACGAAGC TCCATGCAGCTGACAGGCACAGCCATCTTG); GAPDH (TTCCCCA TGGTGTCTGAGCGATGTGGCTCGGCTGGCGACGCAAAAGAAGATG CGGCTGAC).

2.6 | NanoString nCounter assay

The nCounter PanCancer IO 360 Gene Expression Panel (NanoString Technologies), targeting 770 cancer-relevant genes, was used for mRNA expression profiling in BEAS-2B^{circPVT1} and BEAS-2B^{eGFP} (both treated with doxycycline for 48 h). According to the manufacturer's protocol, 100 ng of total RNA from each sample was subjected to nCounter™ SPRINT (NanoString Technologies) analysis, using a 20 h hybridization time. The raw data were processed with the nSOLVER 4.0 software (NanoString Technologies). Positive control normalization was performed as recommended by the manufacturer, using *MRPL19*, *PSMC4*, and *TLK2* reference genes, which showed the lowest coefficient of variance percentage (% CV).

2.7 | xCELLigence proliferation assay

Serial 15-min interval real-time proliferation measurement of cells was performed for 48 h using xCELLigence RTCA DP analyzer (Agilent Technologies) in a cell culture incubator (37°C, 5% CO_2). Using a 16-well electronic microtiter plate (16-PET plate), technical replicates of 2 × 10^4 cells were seeded per condition.

Following the manufacturer's instructions, background measurement was performed using 50 µl of culture medium, then cells were added to a final volume of 100 µl and incubated for 30 min until fully attached.

2.8 | Cell counting

Transfected cells were seeded at 2.5 × 10^5 cells/6-well plate and cultured for 48 h. The percentage of viable cells was determined by Trypan Blue staining (Bio-Rad Laboratories, Inc.) using the TC20 Automated Cell Counter (Bio-Rad Laboratories).

2.9 | Apoptosis assay

Spontaneous apoptosis was assessed by Annexin-V-PE/aminoactinomycin D staining (BD) according to the manufacturer's instructions. The percentage of apoptotic cells was determined by flow cytometry (FACScanto II, BD Biosciences) and analyzed using FACSDiva software (BD Biosciences).

2.10 | Ki67 analysis by flow cytometry

Cells were processed using the Cytofix/Cytoperm kit (BD Biosciences) according to the manufacturer's instructions and stained with the Ki67-Vio667 antibody (Miltenyi Biotec, Bergisch Gladbach, Germany). Flow cytometry analysis was carried out using BD FACSCanto II. Analysis of the percentage of $Ki67^+$ cells and the mean fluorescence intensity was done using the Flowing Software version 2.5.1.

2.11 | Western blotting

Cells were lysed in RIPA buffer (150 mM NaCl, 10 mM Tris–HCl pH 7.2 0.1% SDS, 1.0% Triton X-100, 1% sodium deoxycholate, and 5 mM EDTA). Protein concentrations were determined with the Qubit™ Fluorometer (Thermo Fisher Scientific). Proteins were subjected to gel electrophoresis and Western blotting (WB) as previously described,[51] using the following antibodies: anti-MYC (1:1000),

anti-BCL2 (1:500), and anti-YAP1 (1:1000) (Cell Signaling Technology), anti-POU2F3 (1:1000) (Merck KGaA), anti-NEUROD1 (1:1000) (Abcam), and anti-ASCL1 (1:500) (BD Biosciences). Immuno-reactive bands were detected with anti-mouse and anti-rabbit secondary antibodies conjugated to horseradish peroxidase (HRP) obtained from Santa Cruz Biotechnologies. Signals were detected using Clarity and Clarity Max ECL Western Blotting Substrates (Bio-Rad Laboratories) with Chemidoc System (Bio-Rad Laboratories). Some blots were re-tested to detect a second protein after stripping the revealed antibodies using Restore Western Blot stripping Buffer (Thermo Fisher Scientific). Bands were normalized to total proteins using stain-free technology[52] (Bio-Rad Laboratories). Densitometry analysis was performed using ImageLab (Bio-Rad Laboratories).

2.12 | Polysome profiling

Cytoplasm fractionation on sucrose gradients was performed as follows: briefly, 20×10^6 cells were lysed with 500 µl of lysis buffer (10 mM Tris pH 7.5, 10 mM NaCl, 10 mM $MgCl_2$, 1% Triton X-100, and 0.5% sodium deoxycholate), supplemented with 100 µg/ml cycloheximide, 1X PIC (100 µg/ml) (Complete, EDTA free) (Roche), and 1X RNase guard (Thermo Scientific). The lysates were centrifuged for 5 min at 2000 rpm at 4°C. The supernatants were collected and centrifuged on a 15%–50% sucrose gradient at 37,000 rpm with an SW41 rotor (Beckman) for 2 h at 4°C. Fractions were collected with a Bio-logic LP (Bio-Rad Laboratories). Each fraction (300 µl) was pooled in groups of three samples, obtaining four fractions (HMW, LMW, 80 S, Free RNA).

2.13 | EV RNA isolation

After three PBS washes, BEAS-2B and SCLC cell lines at 70% confluency in T75 cell culture flask were incubated for 48 h in the conditioned medium using Exosome-Depleted FBS Media Supplement (EXO-FBS-250A-1, System Biosciences). EV isolation was performed by using a differential centrifugation protocol.[53] Briefly, a pellet of living cells was obtained after a 5 min centrifugation at 300*g* at 4°C. The supernatant was centrifuged twice for 10 min, respectively at 800*g* and 5,000*g*, to remove cellular debris. Next, EVs were harvested by centrifugation at 15, 000*g* at 4°C for 30 min. The medium was transferred into a new collection tube and ultra-centrifuged at 110,000*g* at 4°C for 70 min. The pellet was resuspended into a large amount of sterile PBS and ultra-centrifuged at 110,000*g* at 4°C for 70 min to remove any protein contamination. We used a Beckman Coulter OPTIMA—XPN 100 ultracentrifuge, TYPE 70 Ti rotor, and 26.3 ml Polycarbonate Bottles (Beckman Coulter; Cat. No. 355618). Finally, the pellet was resuspended in 100 µl sterile PBS 1×.

Size distribution and concentration of isolated EVs were measured by the NanoSight Nanoparticle Tracking Analysis (NTA) (NS300, Malvern Instruments LTD) and reported in Table S4. All experiments were carried out at 1:1000 dilutions and in triplicate. The 60 s video images were acquired and analyzed by the NanoSight NTA 3.2 software.

EV RNA has been extracted with Total Exosome RNA and Protein Isolation Kit (Thermo Fisher Scientific) according to manufacturer's instructions and quantified with Qubit™ Fluorometer (Thermo Fisher Scientific).

2.14 | Statistical analyses

Data are presented as mean ± SD. The paired Student's *t* test was used to compare cell number, apoptosis rate, and protein expression. The Pearson correlation coefficient was calculated between the expression values of *PVT1* and *MYC* in both analyzed GEO data sets. Boxplots were drawn to represent the gene expression values of normal tissues and SCLC tissues relative to individuals exhibiting *MYC* expression higher than the median value within the data set (*MYC* up). All statistical tests were considered significant whenever the *p*-value ≤ 0.05 and were performed using the GraphPad 8.0.1 software (GraphPad Inc.) and R statistical software.

3 | RESULTS

3.1 | *PVT1* transcripts are highly expressed in *MYC*-driven SCLCs

To explore the oncogenic role of *PVT1* in SCLC, particularly in *MYC*-overexpressed cases, we first analyzed publicly available data from SCLC and normal tissues. However, limited data are available as these tumors are rarely excised by surgery, and the aspirated material used for diagnostics is not always adequate for in-depth analysis.[54] We could only find publicly available microarray data for six SCLC tissues (GSE83227) and RNA sequencing of 73 SCLCs (GSE60052). In silico analysis indicated a significant trend toward overexpression of the linear PVT1 (p-value < 0.1) in GSE83227 and a clear statistical difference in GSE60052 (p-value = 0.0045) when considering tumors with *MYC* overexpression versus the healthy counterpart (Figure 1A). Interestingly, both data sets highlighted a significant correlation between the expression values of *MYC* and *PVT1* ($r = 0.87$ and p-value = 0.02; $r = 0.79$ and p-value < 2 e−16; Figure 1B).

Because of the limited data available, we also analyzed a panel of SCLC cell lines to investigate the expression level of PVT1 and circPVT1 by RT-qPCR with primer pairs specifically recognizing each transcript isoform. These analyses revealed a higher expression of circPVT1 and PVT1 versus control in multiple samples, with the highest levels in NCI-H2171 and GLC3 *MYC* amplified cell lines (Figure 1C; Table S1A), pointing toward the accumulation of *PVT1* transcripts as a recurrent event in SCLC, particularly in those ones harboring *MYC* amplification/overexpression.

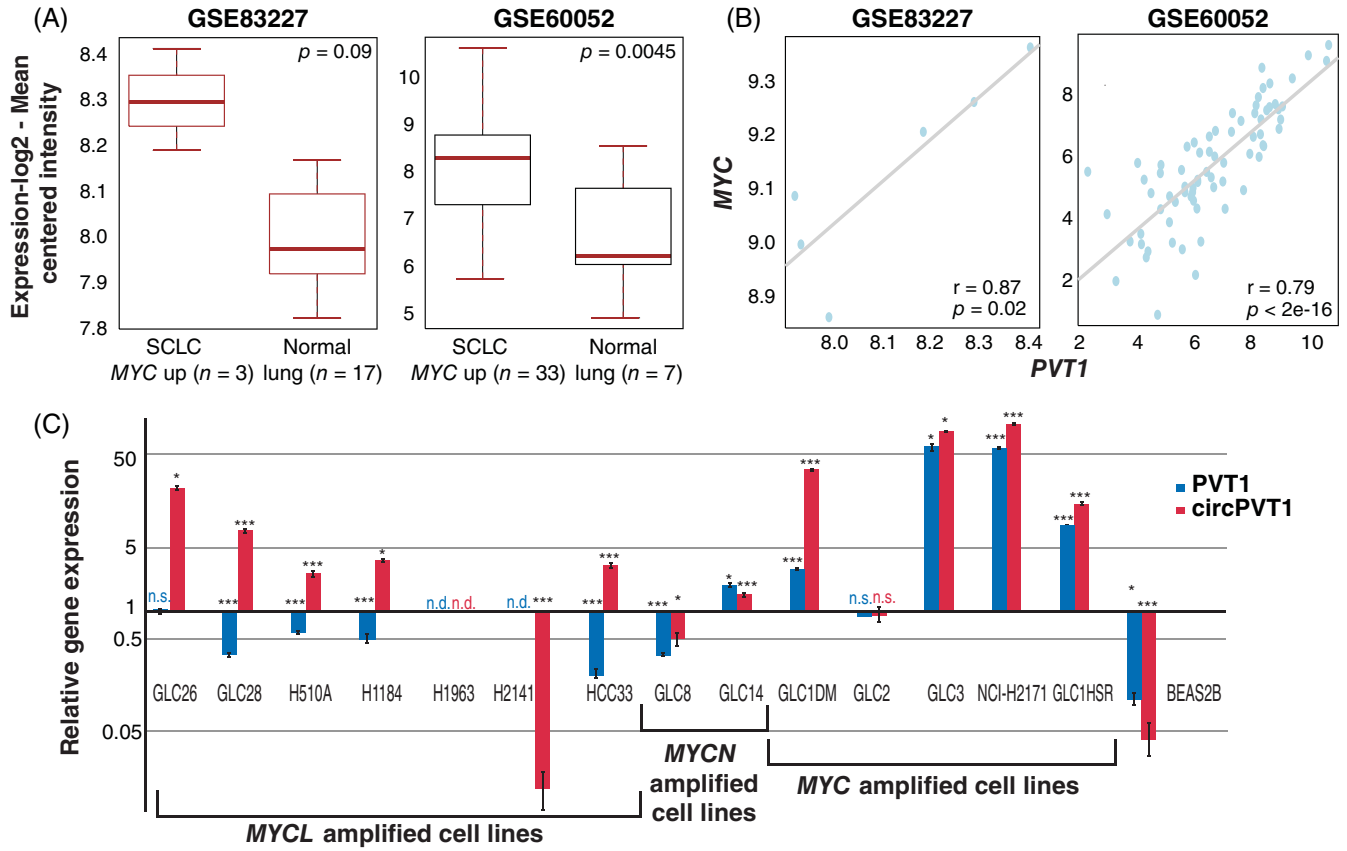

FIGURE 1 PVT1 transcripts are highly expressed in *MYC*-driven SCLCs. (A) Boxplots of RMA-normalized and estimated size factors-normalized PVT1 transcripts for GSE83227 and GSE60052, respectively, of normal lung versus *MYC*-driven SCLCs. (B) Linear regression analysis of PVT1 and *MYC* expression profiles in public data sets. (C) RT-qPCR analyses of PVT1 and circPVT1 in SCLC cell lines using normal lung pooled samples as calibrator (thick black line with value = 1). *p-value < 0.05; ***p-value < 0.001; n.d., not detected; n.s., not significant. p-values are reported in Table S1A. Error bars refer to the SD.

3.2 | circPVT1 stimulates cell proliferation and reduces apoptosis in lung cells

To uncover the molecular phenotype related to circPVT1 overexpression, we generated a model based on the primary lung epithelial cell line BEAS-2B by integrating a doxycycline-inducible circPVT1 expression vector in the genome. Since linear by-products and concatemers are often produced from such vectors,[55,56] we first confirmed that the circular form of *PVT1* was the unique product obtained in our model by Northern blotting (Figure 2A). circPVT1 was significantly overexpressed in the transfected cell line after doxycycline induction versus control, without affecting the linear PVT1 levels (Figure 2B; Table S1B). Gene ontology analysis on a Pan-Cancer NanoString gene expression panel in these engineered cells (Figure S1A), 48 h after doxycycline induction, showed that cellular proliferation and cell cycle regulation were among the top biological processes altered in the circPVT1 overexpressing model (Figure 2C). Indeed, the analysis indicated that several key oncogenes (*MYC*, *MET*) and drivers of cell proliferation (*AXL*, *CCND1*) were upregulated in the circPVT1 overexpressing cells. Conversely, important inhibitors of the cell cycle (*RUNX3*, *CDKN1C*, and *CDKN1A*), as well as the *H2AFX* apoptotic marker gene, were downregulated (Figure 2D; Table S5).

To verify if the observed transcriptional changes translated into an actual phenotype, we evaluated the effects of induced circPVT1 overexpression on cell proliferation by performing an xCELLigence Cell Proliferation Assay.[57] Cells expressing circPVT1 showed a superior proliferative capacity compared with control ones (Figure 2E). Such evidence was corroborated by the significant upregulation of *TPX2*, *TOP2A*, and Ki67 proliferation factors, at mRNA and protein level, respectively, compared with BEAS-2B$^{circPVT1/ND}$ (Figure 2F,G; Table S1C), and an observed positive trend in cell counting induced after doxycycline stimulation (Figure S1B).

Next, to confirm the role of circPVT1 in lung cell proliferation, we investigated the consequences of its transient overexpression in the same cellular model (BEAS-2B$^{circPVT1/48tr}$). Interestingly, circPVT1 displayed a more than twofold expression level in the latter model 48 h after cell transfection compared with BEAS-2B$^{circPVT1/48D}$ (Figure S1C, Table S1B). The significant increase in cell number and expression of proliferation factors was also confirmed in this system compared with its control (BEAS-2B^{CTRL}) (Figure S1D–F, Table S1D).

Besides, increased expression of circPVT1 showed a significant positive impact on the *BCL2* anti-apoptotic factor transcript in all BEAS-2B transfected cell lines (Figure 2H; Figure S1G, Table S1E,F), which came with a significant decrease in the percentage of apoptotic

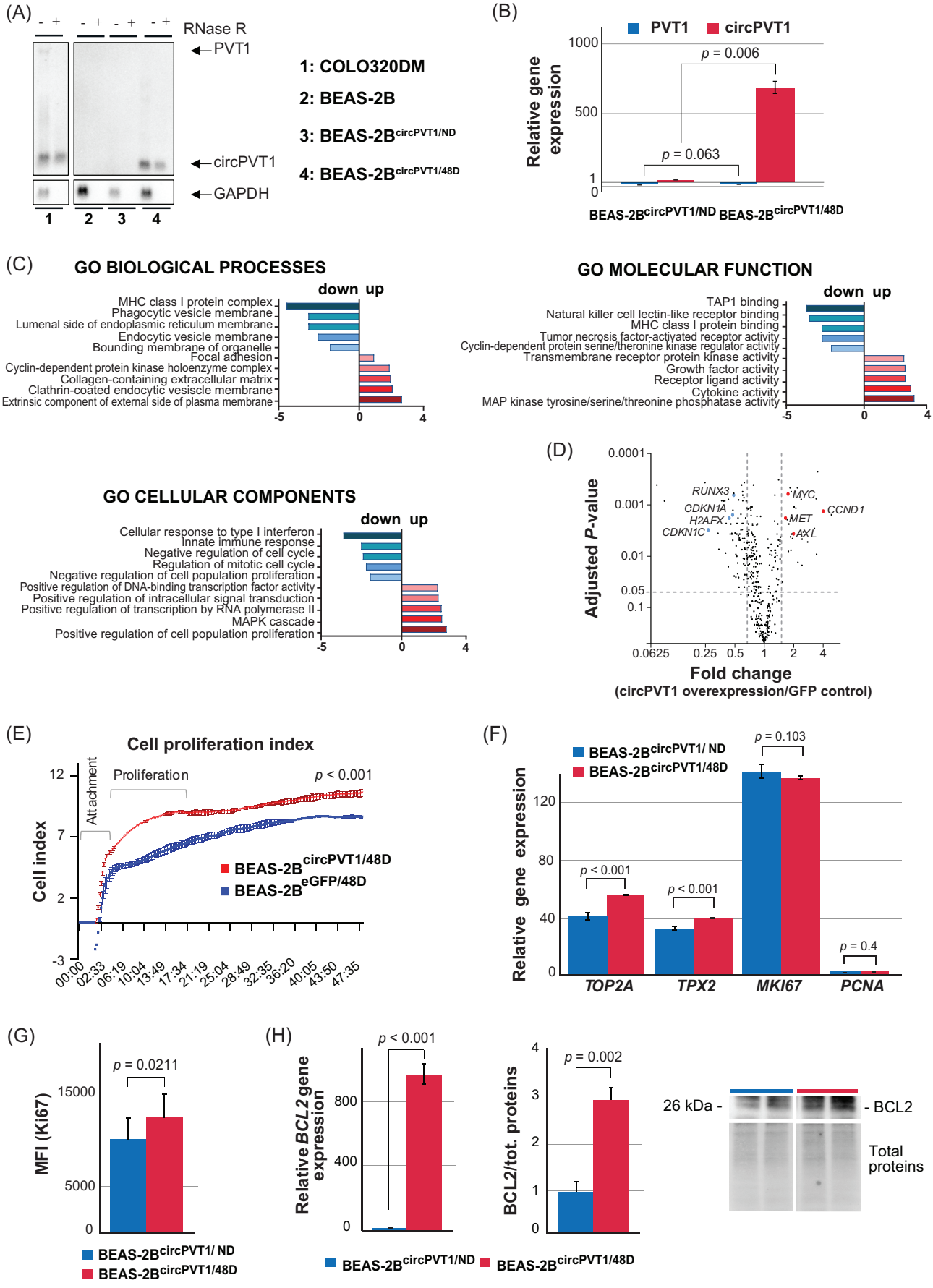

FIGURE 2 Legend on next page.

cells only in BEAS-2B$^{circPVT1/48tr}$ compared with their control (Figure S1H,I).

3.3 | circPVT1 increases MYC and impacts on master regulator gene expression when overexpressed in BEAS-2B cells

The upregulation of *MYC* observed by NanoString analysis is particularly interesting, as it may suggest that a positive feedback loop between circPVT1 and MYC occurs. Therefore, to verify this hypothesis, we examined the impact of circPVT1 expression on MYC. In all BEAS-2B transfected cell lines, both MYC transcript and protein levels were elevated upon circPVT1 overexpression (Figures 3A and S2A, Table S1G,H), highlighting that this circular transcript may cause an accumulation of MYC in SCLC. Moreover, we tested whether circPVT1 regulated the expression of the transcription factors affecting SCLC subtypes. In both BEAS-2B$^{circPVT1/48D}$ and BEAS-2B$^{circPVT1/48tr}$, significant overexpression of YAP1 (Figures 3B and S2B) as well as a decrease of POU2F3 (Figures 3C and S2C), was observed upon increased circPVT1 expression. No difference was detected in the expression of ASCL1 and NEUROD1 (Figure S2D–G).

Overall, the data may suggest a specific implication of circPVT1 on SCLC-Y and -P by altering MYC, YAP1, and POU2F3 expression levels. To verify if the effect on YAP1 and POU2F3 might be MYC-dependent, we performed MYC knockdown by RNA interference. After assessing the significant downregulation of MYC in BEAS-2B$^{circPVT1/48D}$ transfected with siRNA2 *MYC* versus an appropriate control sample (the same cell line transfected with the si-NC) by RT-qPCR (Figure 3D; Table S1I) and WB (Figure 3E), we observed no effect on YAP1 (Figure 3F) and an increase of POU2F3 protein (Figure 3G). This result may indicate a MYC-independent impact of circPVT1 on YAP1 and a possible interaction between MYC and POU2F3.

3.4 | circPVT1 does not show protein-coding activity

To further define the role of circPVT1, we evaluated its protein-coding potential by polysome fractionation, followed by RT-PCR using circPVT1-specific primers. These experiments were performed in GLC3 cells, showing high endogenous expression of circPVT1 (Figure 1C; Table S1A). The results indicated an association of circPVT1 with high-molecular-weight polysomes (HMW), low-molecular-weight polysomes (LMW), and 80 S polysomes in GLC3 (Figure 4A). Hence, we tested whether the longest predicted circPVT1 ORF, encompassing the back-splicing junction, fused with the FLAG-tag, may encode a peptide. However, WB analyses in HeLa cells transfected with the FLAG-tagged circPVT1 ORF did not reveal any protein product (Figure 4B), indicating that circPVT1 is unlikely to have protein-coding activity.

3.5 | chimPVT1 shows a tumorigenic role in vitro

To investigate the tumorigenic potential of *PVT1* chimeric transcripts in SCLC, we focused on chimPVT1, previously identified and validated in the GLC1HSR cell line,[22] targeting its fusion junction by a specific shRNA knockdown.

chimPVT1 downregulation was established in the GLC1HSR cell line (GLC1HSR^{shchimPVT1}) (Figure 5A; Table S1J) and impacted the cell phenotype. We observed a significant decrease in cell growth in GLC1HSR^{shchimPVT1} compared with GLC1HSR^{Scram} (Figure 5B). These results were corroborated by the downregulation at transcript level of key cell cycle markers (i.e., *TOP2A*, *TPX2*, *MKI67*, and *PCNA*) (Figure 5C; Table S1K) in GLC1HSR^{shchimPVT1}. A negative trend was also observed in the flow cytometry analysis of Ki67 expression (Figure S3A). Furthermore, we observed a decreased *BCL2* expression at the transcript level and an increased apoptosis rate in GLC1HSR^{shchimPVT1} compared with GLC1HSR^{Scram} (Figure 5D,E; Table S1L). Interestingly, downregulation of the chimera significantly decreased MYC (both at transcript and protein level) and circPVT1 while showing no effect on PVT1 (Figure 5F,G; Table S1M) and wild-type *AKT3* (Figure 5H; Table S1N). Moreover, WB analysis of the lineage-specific transcriptional factors revealed a significant decrease of YAP1 and POU2F3 (Figure 5I,J), whereas no difference was observed for NEUROD1 and ASCL1 (Figure S3B,C).

Overall, these findings highlight chimPVT1 as a pro-oncogenic factor in SCLC.

FIGURE 2 circPVT1 stimulates cell proliferation factors and BCL2 expression. (A, B) Northern blot and RT-qPCR analyses of BEAS-2B cells overexpressing circPVT1 after 48 h of doxycycline induction, showing no effect on linear PVT1. For Northern blot, a probe targeting PVT1 exon 2 was used. In (A) COLO320DM cell line harboring the amplification of *PVT1* exon 2 and overexpressing circPVT1 is used as a positive control, while *GAPDH* is used as a housekeeping linear RNA control. In (B), a normal lung pooled sample was used as a calibrator. Error bars refer to SD. (C) List of enriched gene ontology biological processes, GO cellular components, and GO molecular functions from the deregulated set of genes depicted in D. (D) Volcano plot showing the differential expression values from the nanostring pan-cancer panel 48 h after the doxycycline-mediated induction of circPVT1 on BEAS-2B$^{circPVT1/48D}$ cells. Down- and upregulated cell cycle and proliferation-related genes are highlighted in blue and red, respectively. (E) Cell proliferation index assay measured for 2 days (every 15 min) after 48 h of circPVT1 doxycycline-induction in the BEAS-2B$^{circPVT1/48D}$ model versus control. Attachment period lasted ~2 h prior to proliferation starts. (F) RT-qPCR analyses showing the expression levels of *TOP2A*, *TPX2*, *MKI67*, and *PCNA* on BEAS-2B^{circPVT1} with and without doxycycline induction, using a normal lung pooled sample as calibrator. (G) Ki67 evaluation by flow cytometry. MFI, mean fluorescent intensity. (H) BCL2 transcript (left panel) and protein (right panel) evaluation following the induction (at 48 h) of circPVT1. The RT-qPCR assay was performed using the BEAS-2B$^{circPVT1/ND}$ cells as a calibrator. WB histograms show the normalized values obtained using three biological replicates, +/− SD. One representative replicate blot is shown. In (B), (E–H), error bars refer to SD.

3.6 | *PVT1* transcripts are secreted into EVs from SCLC cell lines

Finally, we tested the potential secretion of *PVT1* transcripts into EVs from SCLC cell lines. RT-qPCR showed the highest level of circPVT1 and PVT1 secretion in EVs from tested cell lines harboring the *MYC* genomic amplification (GLC3 and GLC1HSR), as well as in one cell line (H510A) with *MYCL* amplification (Figure 6A; Table S1O). Conversely, no secretion was observed in EVs from BEAS-2B cells.

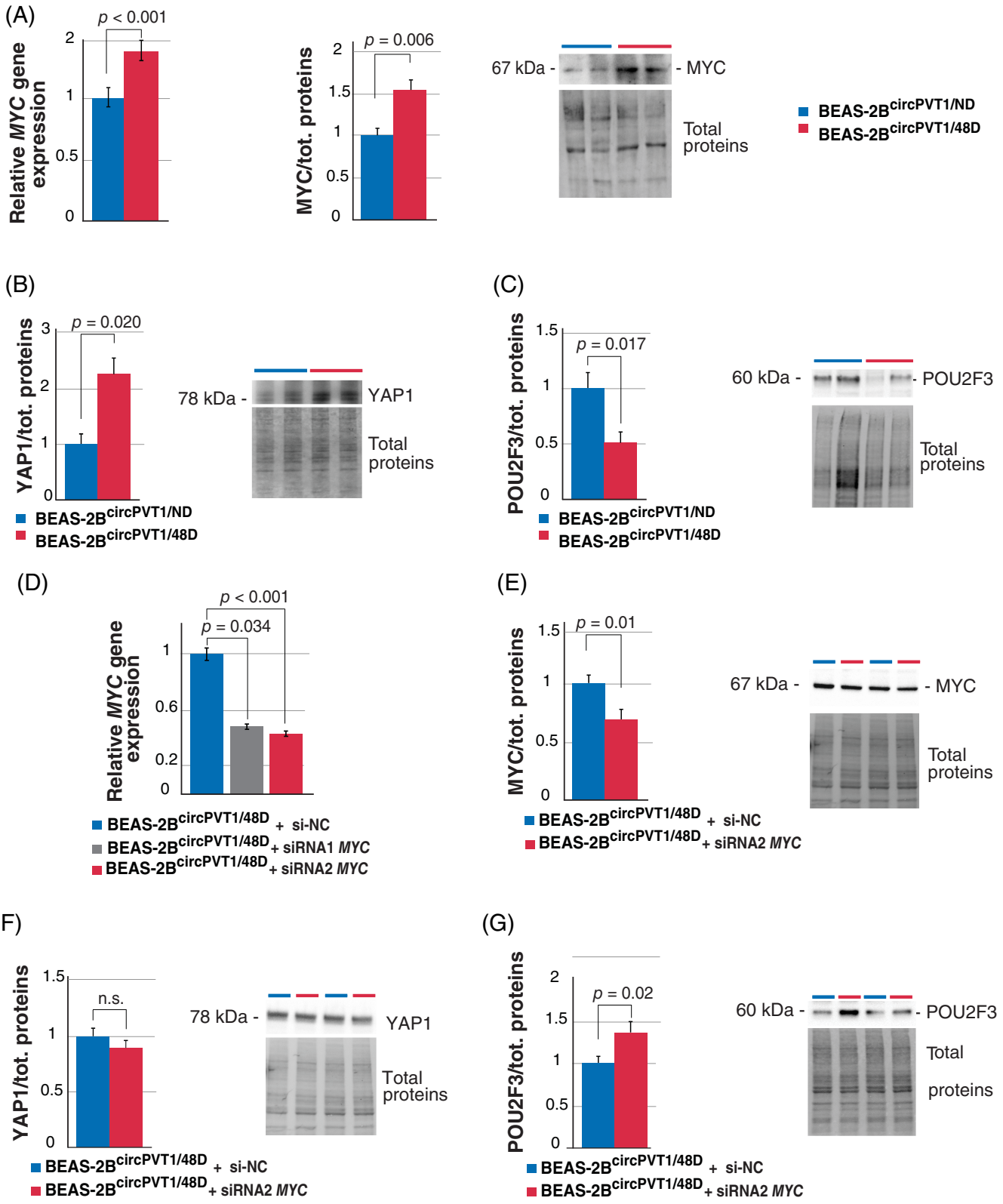

FIGURE 3 Legend on next page.

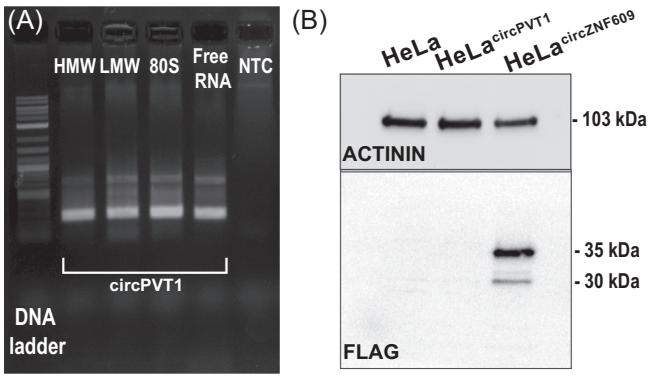

FIGURE 4 Analysis of the translational potential of circPVT1. (A) RT-qPCR analyses of circPVT1 in high-molecular-weight polysomes (HMW) and low-molecular-weight polysomes (LMW), in 80 S ribosomes, free RNA, and control without RNA (NTC). The 2-Log DNA ladder (New England Biolabs) was used as a DNA molecular weight marker. (B) WB with an anti-FLAG antibody in HeLa cells, transfected with a vector expressing the longest circPVT1 ORF in frame with the FLAG tag (HeLa^{circPVT1}), and expressing (as positive control) the circZNF609 ORF in frame with the FLAG tag (HeLa^{circZNF609}). On the top panel, actinin is used as a positive control.

Notably, chimPVT1 was detected in secreted EVs, as shown by RT-PCR experiments and Sanger sequencing on GLC1HSR EV RNA (Figure 6B).

4 | DISCUSSION

We speculated that unconventional transcripts (circRNAs and chimeras) originating from *PVT1* could be key drivers of SCLC tumorigenesis and may be used as biomarkers for *MYC*-driven SCLCs.

In the present work, in silico analysis indicated a significant correlation between *PVT1* and *MYC* expression in SCLC patients. This result was corroborated in SCLC cell lines, where the highest PVT1 expression levels were observed in *MYC*-amplified cell lines. In addition, we found circPVT1 overexpression in SCLC cell lines, with the highest level in samples with *MYC* and *PVT1* amplification.[22,44] Our results suggest that SCLC might be accompanied by the accumulation of circPVT1, which may provide an essential contribution to lung tumorigenesis. Even though obtained in cell lines, this result is particularly relevant considering that circPVT1 has never been investigated in SCLC before. Data on its tumorigenic role and as a prognostic biomarker are only available in NSCLC[23,58–62] among lung cancer types. A Pan-Cancer gene panel expression analysis, corroborated by cell proliferation and apoptosis assays of circPVT1-overexpressing models, indicated a clear overlap between the molecular and cellular phenotypes induced upon enrichment of this circRNA.

Furthermore, we did not observe any impact of circPVT1 overexpression on its linear counterpart. As a matter of fact, the two molecules are transcribed by different promoters, enriched into different cellular domains (PVT1 and circPVT1 in the nucleus and the cytoplasm, respectively), and show a poor correlation in their expression levels.[34,63,64] Overall, such evidence confirms that the two transcripts of *PVT1* behave as separate entities within tumor cells.

Concerning MYC, its expression was significantly increased in all circPVT1-overexpressing models, indicating positive feedback on this multifaceted oncogene. Our evidence aligns with previous reports in gastric cancer,[63] acute lymphocytic leukemia,[65] and prostate cancer.[66] The "circPVT1-MYC" axis[67] could be explained by a circPVT1 sponging activity toward the let-7 miRNA,[68] known as a negative translational regulator of MYC and recently also demonstrated for two other let-7 targets, NRAS, and HMGA2.[61]

A similar effect was also observed on the *BCL2* gene encoding the BCL2 anti-apoptotic protein, as already documented in breast cancer,[69] acute lymphocytic leukemia,[65] and NSCLC.[23]

Notably, circPVT1 overexpression induced YAP1 and decreased POU2F3, master regulator genes in SCLC, respectively defining SCLC-Y and SCLC-P subtypes, the former with a more significant benefit from the addition of immunotherapy to chemotherapy than the latter.[12] Interestingly, MYC knockdown indicated no effect on YAP1, reinforcing the hypothesis concerning a direct impact of circPVT1 on YAP1. This result opens new scenarios on the role of circPVT1 in the definition of SCLC subtypes. The "YAP-circPVT1" regulatory loop, if also confirmed in patients, might open a window for the development of new treatment options in SCLC, considering that a series of small-molecule modulators of YAP1, the key transcriptional regulator in the Hippo pathway, has been used in clinical trials.[70] Moreover, YAP1 expression has been recently described as involved in chemoresistance.[71] Interestingly, given the sober prognosis of SCLC, patient stratification and identification of druggable targets could hold promise to narrow the gap between the lab bench and bedside.

So far, the oncogenic role of circPVT1 has mainly been attributed to its function as a miRNA sponge.[72] It has been described to act as a sponge for a plethora of miRNAs, regulating the activities of PI3K/AKT, Wnt5a/Ror2, E2F2, and HIF-1α.[73] Hence, we explored a novel potential function as protein-coding RNA, already documented

FIGURE 3 Evaluation of MYC, YAP1, and POU2F3 protein expression in BEAS-2B cells after circPVT1 stable overexpression and MYC knockdown. (A) RT-qPCR (left panel, using BEAS-2B$^{circPVT1/ND}$ cells as calibrator sample) and WB (right panel) analyses of MYC after the stable overexpression of circPVT1. (B, C) WB analyses of YAP1 (B) and POU2F3 (C) were conducted 48 h after doxycycline induction in BEAS-2B$^{circPVT1/48D}$ cells versus control. (D, E) Evaluation of MYC knockdown. (D) RT-qPCR experiments 24 h after transfection of BEAS-2B$^{circPVT1/48D}$ with siRNA1 *MYC* and siRNA2 *MYC* versus the cell line transfected with the si-NC (used as calibrator). (E) WB analyses of MYC 48 h after the transfection with siRNA2 *MYC*. (F, G) WB analyses of YAP1 (F) and POU2F3 (G) in BEAS-2B$^{circPVT1/48D}$ cells with MYC knockdown versus control. The immunoblotting membrane in E was subject to stripping to detect YAP1 in F. All WB histograms show the normalized values obtained using three biological replicates, +/− SD. One representative replicate blot is shown. In RT-qPCR and WB assays, error bars refer to SD.

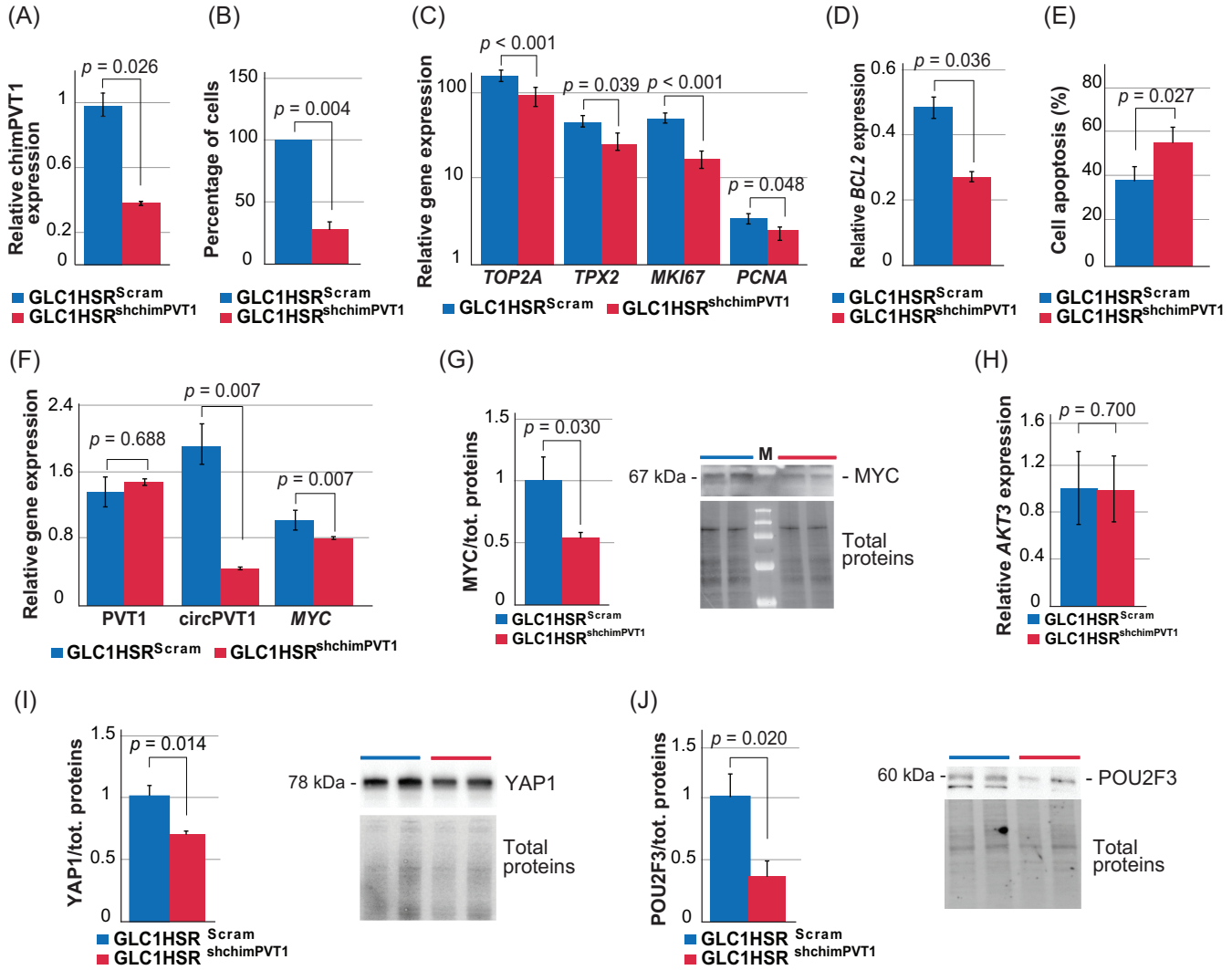

FIGURE 5 In vitro analysis of the oncogenic effect of chimPVT1 expression in GLC1HSR cell line. (A) RT-qPCR evaluation of chimPVT1 downregulation in GLC1HSR^{shchimPVT1} versus GLC1HSR^{Scram}. (B) Cell count results after chimPVT1 knockdown. The histogram shows the percentage of GLC1HSR^{shchimPVT1} cells relative to GLC1HSR^{Scram} cells (100%). (C) RT-qPCR assays displaying a reduction of *TOP2A*, *TPX2*, *MKI67*, and *PCNA* gene expression after GLC1HSR transfection with the chimPVT1 shRNA. (D) RT-qPCR results showing a significant reduction of *BCL2* at the transcript level in GLC1HSR^{shchimPVT1} versus GLC1HSR^{Scram}. (E) Flow cytometry assay showing apoptosis (% of Annexin-V^{+} cells) increase in GLC1HSR^{shchimPVT1} versus GLC1HSR^{Scram}. (F) RT-qPCR assays showing no impact of chimPVT1 on PVT1 expression but a significant negative effect on circPVT1 and *MYC*. (G) The result on MYC was corroborated at the protein level by WB analysis. (H) RT-qPCR assay demonstrating that wild-type *AKT3* expression is not affected by chimPVT1 shRNA silencing. (I, J) WB analyses indicate a significant effect on YAP1 (I) and POU2F3 (J) master regulator proteins in GLC1HSR^{shchimPVT1} versus GLC1HSR^{Scram}. All WB histograms show the normalized values obtained in three biological replicates, +/− SD. One representative membrane is shown. (M) PageRuler Plus Prestained Protein Ladder (ThermoFisher Scientific). The immunoblotting membrane in J was subject to stripping to detect NEUROD1 in Figure S3B. The RT-qPCR assays were performed using a normal lung pooled sample as a calibrator (Table S1J–N). In RT-qPCR and WB assays, error bars refer to SD.

for other circRNAs.[50,74,75] Despite of the presence of an internal 104 aa ORF[72] crossing the back-splicing junction and the detected association of circPVT1 with HMW, LMW, and 80 S polysomes, we could not identify any translated product using immunodetection of the tagged protein. Further studies are required to explain the co-localization of circPVT1 with polysomes, reported here for the first time. Moreover, the presence of lncPVT1 and circPVT1 in EVs secreted from SCLC cell lines and their absence in BEAS-2B cells suggest that both transcripts may exert important functions in tumor biology and therapy resistance, in line with previous evidence in other cancer types.[76,77] Importantly, the excretion of circPVT1 in exosomes is described to contribute to cisplatin resistance by regulating autophagy, invasion, and apoptosis via miR-30a-5p/YAP1 axis in gastric cancer.[76]

Regarding the chimeric transcripts involving the *PVT1* gene, despite being described in multiple cancer types,[35,44,78,79] to the best of our knowledge, their oncogenic role was neglected thus far, with the only exception of *PVT1/MYC* in medulloblastoma.[80] The in vitro

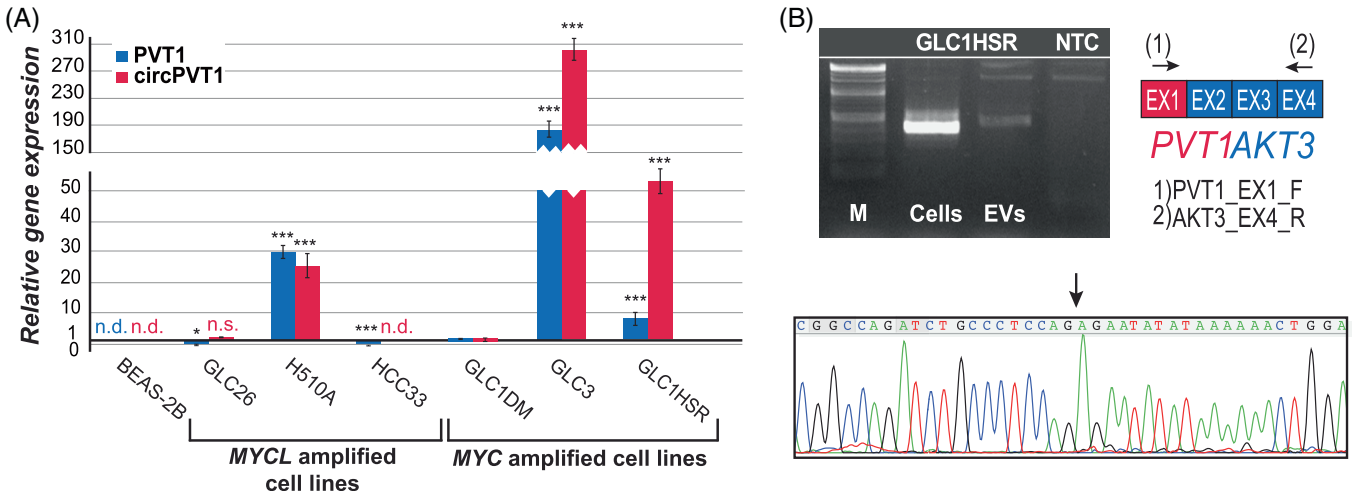

FIGURE 6 PVT1 transcripts are secreted into EVs. (A) RT-qPCR analysis of PVT1 and circPVT1 in EVs isolated from SCLC cell lines. EV RNA from the GLC1DM cell line was used as a calibrator sample (thick black line, value = 1). *p*-values are reported in Table S1O. Error bars refer to SD. **p*-value < 0.05; ****p*-value < 0.001; n.d., not detected; n.s., not significant. (B) Top left panel: RT-PCR evaluation of the chimPVT1 transcript, using the PVT1_Ex1_F + AKT3_EX4R primer pair (Table S2), on RNA extracted from EVs secreted by the GLC1HSR cell line (EVs) and from the corresponding cell line of origin (Cells). (M) DNA ladder (2-Log DNA Ladder, New England Biolabs). NTC, PCR no-template control. The RT-PCR product corresponds to the fusion junction between *5′PVT1* and *3′AKT3*, as shown by the schematic representation of the chimeric transcript (top right panel). The black arrows indicate the used primer pair. Bottom panel: partial chromatogram showing the obtained *PVT1/AKT3* fusion PCR product. The black arrow points to the fusion junction between *PVT1* and *AKT3*.

downregulation of chimPVT1 led to a decreased cell proliferation and an increased apoptosis rate. Notably, downregulation of MYC, circPVT1, YAP1, and POU2F3 was also observed, suggesting a potentially intriguing network involving *MYC*, circular, and chimeric *PVT1* RNAs, and these transcription factors. Thus, our results suggest that *PVT1* fusion transcripts may have an oncogenic function and contribute to SCLC carcinogenesis. As such transcripts are often described as accompanying the genomic amplification of *PVT1*,[36] our findings add the notion of chimeras as pathogenic actors in such tumors.[81,82] Genomic amplification may have a twofold impact on cancer cells, that is, activating amplified genes (*MYC* in the investigated tumors) and generating chimeric transcripts with oncogenic potential.

Lastly, we found that, like circPVT1 and PVT1, chimPVT1 is also wrapped within EVs isolated from the SCLC cell lines. Although further studies on the *PVT1* transcripts in patient body fluids are needed, the early detection of such molecules in EVs from patient blood in prospective studies could pave the way for the development of new tools for the noninvasive diagnosis, prognostication, and follow-up of at least a subset of SCLC patients, as already proposed for other transcripts in cancer.[83,84]

Overall, our results suggest that circular and chimeric *PVT1* RNAs may provide a pivotal contribution to SCLC tumorigenesis, mostly in tumors with *MYC* amplification/overexpression, and the definition of tumor subtypes, with distinct molecular and biological features. We showed that circPVT1 and chimPVT1 have an oncogenic impact in vitro by promoting lung cell proliferation and inhibiting apoptosis. Our results were obtained using novel cell models for the study of circular and chimeric PVT1 transcripts in lung cancer. These cell models could be an important resource for the scientific community to further investigate the biological role of PVT1 transcripts.

Furthermore, both transcripts revealed a positive effect on MYC, *BCL2*, and YAP1, never described so far in SCLC. circPVT1 was also shown to decrease POU2F3, while the chimPVT1 indicated a positive impact on POU2F3. Considering the recent classification based on the four lineage-specific master regulators, such evidence suggests a role of *PVT1* transcripts in the subtype definition of SCLCs. Our results, which need to be confirmed using in vivo models, open new scenarios toward identifying new biomarkers in this cancer type, considering their inclusion into secreted EVs. These findings are novel and important for overcoming the current "monolithic" therapeutic approach for SCLCs, paving the way toward the achievement of personalized treatments.

ACKNOWLEDGMENTS

We thank Dr. Kimberly A. Nevonen for the English editing of the manuscript. The graphical abstract was created with BioRender.com. This work was supported by the AIRC (Associazione Italiana per la Ricerca sul Cancro, AIRC IG no. 25706 to Clelia Tiziana Storlazzi) and by the PON AIM (Programma Operativo Nazionale Attrazione e Mobilità Internazionale, no. 1807508-2), supporting Doron Tolomeo.

CONFLICT OF INTEREST

Giovanni Martinelli has the following conflict of interests: consultant/advisor/speaker bureau of Abbvie; Incyte; Pfizer; Celgene/BMS; Amgen, Roche; GlaxoSmithKline; Astellas; Daiichi Sankyo; Takeda; Janssen; Servier. Research support from: Pfizer, AbbVie, AstraZeneca, Daiichi Sankyo, Takeda, and Ariad/Incyte. The other authors have no conflict of interest to disclose.

DATA AVAILABILITY STATEMENT

The data that supports the findings of this study are available in the supplementary material of this article.

ORCID

Debora Traversa https://orcid.org/0000-0003-0030-2394
Juan L. García Rodríguez https://orcid.org/0000-0002-1818-1781
René Massimiliano Marsano https://orcid.org/0000-0001-8450-1010
Clelia Tiziana Storlazzi https://orcid.org/0000-0002-1696-0028

REFERENCES

1. Howlader N, Noone AM, Krapcho M, et al. *SEER Cancer Statistics Review, 1975–2016*. 2019.
2. Mathieu L, Shah S, Pai-Scherf L, et al. FDA approval summary: atezolizumab and durvalumab in combination with platinum-based chemotherapy in extensive stage small cell lung cancer. *Oncologist*. 2021;26(5):433-438.
3. Smith KER, Mansfield AS. Validating chemoimmunotherapy in small-cell lung cancer. *Lancet Oncol*. 2022;23(6):692-693.
4. Horn L, Mansfield AS, Szczęsna A, et al. First-line atezolizumab plus chemotherapy in extensive-stage small-cell lung cancer. *N Engl J Med*. 2018;379(23):2220-2229.
5. Paz-Ares L, Dvorkin M, Chen Y, et al. Durvalumab plus platinum–etoposide versus platinum–etoposide in first-line treatment of extensive-stage small-cell lung cancer (CASPIAN): a randomised, controlled, open-label, phase 3 trial. *Lancet*. 2019;394(10212):1929-1939.
6. Cheng Y, Han L, Wu L, et al. Effect of first-line Serplulimab vs placebo added to chemotherapy on survival in patients with extensive-stage small cell lung cancer: the ASTRUM-005 randomized clinical trial. *JAMA*. 2022;328(12):1223-1232.
7. Wang J, Zhou C, Yao W, et al. Adebrelimab or placebo plus carboplatin and etoposide as first-line treatment for extensive-stage small-cell lung cancer (CAPSTONE-1): a multicentre, randomised, double-blind, placebo-controlled, phase 3 trial. *Lancet Oncol*. 2022;23(6):739-747.
8. Ionova Y, Vuong W, Sandoval O, et al. Cost-effectiveness analysis of Atezolizumab versus Durvalumab as first-line treatment of extensive-stage small-cell lung cancer in the USA. *Clin Drug Investig*. 2022;42(6):491-500.
9. Mollaoglu G, Guthrie MR, Böhm S, et al. MYC drives progression of small cell lung cancer to a variant neuroendocrine subtype with vulnerability to aurora kinase inhibition. *Cancer Cell*. 2017;31(2):270-285.
10. Rudin CM, Poirier JT, Byers LA, et al. Molecular subtypes of small cell lung cancer: a synthesis of human and mouse model data. *Nat Rev Cancer*. 2019;19(5):289-297.
11. Huang YH, Klingbeil O, He XY, et al. POU2F3 is a master regulator of a tuft cell-like variant of small cell lung cancer. *Genes Dev*. 2018;32(13–14):915-928.
12. Gay CM, Stewart CA, Park EM, et al. Patterns of transcription factor programs and immune pathway activation define four major subtypes of SCLC with distinct therapeutic vulnerabilities. *Cancer Cell*. 2021;39(3):346-360.e7.
13. Plaja A, Moran T, Carcereny E, et al. Small-cell lung cancer Long-term survivor patients: how to find a needle in a haystack? *Int J Mol Sci*. 2021;22(24):13508.
14. Owonikoko TK, Niu H, Nackaerts K, et al. Randomized phase II study of paclitaxel plus alisertib versus paclitaxel plus placebo as second-line therapy for SCLC: primary and correlative biomarker analyses. *J Thorac Oncol*. 2020;15(2):274-287.
15. Dammert MA, Brägelmann J, Olsen RR, et al. MYC paralog-dependent apoptotic priming orchestrates a spectrum of vulnerabilities in small cell lung cancer. *Nat Commun*. 2019;10(1):3485.
16. Chalishazar MD, Wait SJ, Huang F, et al. MYC-driven small-cell lung cancer is metabolically distinct and vulnerable to arginine depletion. *Clin Cancer Res*. 2019;25(16):5107-5121.
17. Peifer M, Fernández-Cuesta L, Sos ML, et al. Integrative genome analyses identify key somatic driver mutations of small-cell lung cancer. *Nat Genet*. 2012;44:1104-1110. doi:10.1038/ng.2396
18. Ireland AS, Micinski AM, Kastner DW, et al. MYC drives temporal evolution of small cell lung cancer subtypes by reprogramming neuroendocrine fate. *Cancer Cell*. 2020;38(1):60-78.e12.
19. Massó-Vallés D, Beaulieu ME, Soucek L. MYC, MYCL, and MYCN as therapeutic targets in lung cancer. *Expert Opin Ther Targets*. 2020;24(2):101-114.
20. Fiorentino FP, Marchesi I, Schröder C, Schmidt R, Yokota J, Bagella L. BET-inhibitor I-BET762 and PARP-inhibitor talazoparib synergy in small cell lung cancer cells. *Int J Mol Sci*. 2020;21(24):1-16.
21. Patel AS, Yoo S, Kong R, et al. Prototypical oncogene family Myc defines unappreciated distinct lineage states of small cell lung cancer. *Sci Adv*. 2021;7(5):eabc2578.
22. L'Abbate A, Macchia G, D'Addabbo P, et al. Genomic organization and evolution of double minutes/homogeneously staining regions with MYC amplification in human cancer. *Nucleic Acids Res*. 2014;42(14):9131-9145.
23. Qin S, Zhao Y, Lim G, Lin H, Zhang X, Zhang X. Circular RNA PVT1 acts as a competing endogenous RNA for miR-497 in promoting non-small cell lung cancer progression. *Biomed Pharmacother*. 2019;111:244-250.
24. Li X, Zhang Z, Jiang H, et al. Circular RNA circPVT1 promotes proliferation and invasion through sponging miR-125b and activating E2F2 signaling in non-small cell lung cancer. *Cell Physiol Biochem*. 2018;51(5):2324-2340.
25. Xi Y, Shen W, Jin C, Wang L, Yu B. PVT1 promotes the proliferation and migration of non-small cell lung cancer via regulating miR-148/RAB34 signal axis. *Onco Targets Ther*. 2020;13:1819-1832.
26. Yang YR, Zang SZ, Zhong CL, Li YX, Zhao SS, Feng XJ. Increased expression of the lncRNA PVT1 promotes tumorigenesis in non-small cell lung cancer. *Int J Clin Exp Pathol*. 2014;7(10):6929-6935.
27. Wu D, Li Y, Zhang H, Hu X. Knockdown of Lncrna PVT1 enhances radiosensitivity in non-small cell lung cancer by sponging miR-195. *Cell Physiol Biochem*. 2017;42(6):2453-2466.
28. Cui D, Yu CH, Liu M, Xia QQ, Zhang YF, Jiang WL. Long non-coding RNA PVT1 as a novel biomarker for diagnosis and prognosis of non-small cell lung cancer. *Tumor Biol*. 2016;37(3):4127-4134.
29. Wan L, Sun M, Liu GJ, et al. Long noncoding RNA PVT1 promotes non-small cell lung cancer cell proliferation through epigenetically regulating LATS2 expression. *Mol Cancer Ther*. 2016;15(5):1082-1094.
30. Wang D, Hu Y. Long non-coding RNA PVT1 competitively binds MicroRNA-424-5p to regulate CARM1 in Radiosensitivity of non-small-cell lung cancer. *Mol Ther Nucleic Acids*. 2019;16:130-140.
31. Qi G, Li L. Long non-coding RNA PVT1 contributes to cell growth and metastasis in non-small-cell lung cancer by regulating miR-361-3p/SOX9 axis and activating Wnt/β-catenin signaling pathway. *Biomed Pharmacother*. 2020;126:110100.
32. Guo D, Wang Y, Ren K, Han X. Knockdown of LncRNA PVT1 inhibits tumorigenesis in non-small-cell lung cancer by regulating miR-497 expression. *Exp Cell Res*. 2018;362(1):172-179.
33. Qiu C, Li S, Sun D, Yang S. LncRNA PVT1 accelerates progression of non-small cell lung cancer via targeting miRNA-526b/EZH2 regulatory loop. *Oncol Lett*. 2020;19(2):1267-1272.
34. Traversa D, Simonetti G, Tolomeo D, et al. Unraveling similarities and differences in the role of circular and linear PVT1 in cancer and human disease. *Br J Cancer*. 2021;126(6):835-850.

35. Iwakawa R, Takenaka M, Kohno T, et al. Genome-wide identification of genes with amplification and/or fusion in small cell lung cancer. *Genes Chromosomes Cancer*. 2013;52(9):802-816.
36. Tolomeo D, Agostini A, Visci G, Traversa D, Storlazzi CT. PVT1: a long non-coding RNA recurrently involved in neoplasia-associated fusion transcripts. *Gene*. 2021;779:145497. doi:10.1016/j.gene.2021.145497
37. Trombetta D, Graziano P, Scarpa A, et al. Frequent NRG1 fusions in Caucasian pulmonary mucinous adenocarcinoma predicted by Phospho-ErbB3 expression. *Oncotarget*. 2018;9(11):9661-9671.
38. Ciampricotti M, Karakousi T, Richards AL, et al. Rlf-Mycl gene fusion drives tumorigenesis and metastasis in a mouse model of small cell lung cancer. *Cancer Discov*. 2021;11(12):3214-3229.
39. Jin K, Wang S, Zhang Y, et al. Long non-coding RNA PVT1 interacts with MYC and its downstream molecules to synergistically promote tumorigenesis. *Cell Mol Life Sci*. 2019;76(21):4275-4289.
40. Huang C, Liu S, Wang H, Zhang Z, Yang Q, Gao F. LncRNA PVT1 overexpression is a poor prognostic biomarker and regulates migration and invasion in small cell lung cancer. *Am J Transl Res*. 2016;8(11):5025-5034.
41. Dobin A, Davis CA, Schlesinger F, et al. STAR: ultrafast universal RNA-seq aligner. *Bioinformatics*. 2013;29(1):15-21.
42. Love MI, Huber W, Anders S. Moderated estimation of fold change and dispersion for RNA-seq data with DESeq2. *Genome Biol*. 2014;15(12):550.
43. Storlazzi CT, Lonoce A, Guastadisegni MC, et al. Gene amplification as doubleminutes or homogeneously staining regions in solid tumors: origin and structure. *Genome Res*. 2010;20(9):1198-1206.
44. Pleasance ED, Stephens PJ, O'Meara S, et al. A small-cell lung cancer genome with complex signatures of tobacco exposure. *Nature*. 2010;463(7278):184-190.
45. L'Abbate A, Tolomeo D, Cifola I, et al. MYC-containing amplicons in acute myeloid leukemia: genomic structures, evolution, and transcriptional consequences. *Leukemia*. 2018;32(10):2152-2166.
46. Macchia G, Severgnini M, Purgato S, et al. The hidden genomic and transcriptomic plasticity of giant marker chromosomes in cancer. *Genetics*. 2018;208(3):951-961.
47. Vandesompele J, De Preter K, Pattyn F, et al. Accurate normalization of real-time quantitative RT-PCR data by geometric averaging of multiple internal control genes. *Genome Biol*. 2002;3(7):research0034.1.
48. Pfaffl MW, Horgan GW, Dempfle L. Relative expression software tool (REST) for group-wise comparison and statistical analysis of relative expression results in real-time PCR. *Nucleic Acids Res*. 2002;30(9):36e-336e.
49. Xiang X, Yuan D, Liu Y, et al. PIM1 overexpression in T-cell lymphomas protects tumor cells from apoptosis and confers doxorubicin resistance by upregulating c-myc expression. *Acta Biochim Biophys Sin Shanghai*. 2018;50(8):800-806.
50. Legnini I, Di Timoteo G, Rossi F, et al. Circ-ZNF609 is a circular RNA that Can Be translated and functions in myogenesis. *Mol Cell*. 2017;66(1):22-37.e9.
51. Centrone M, Ranieri M, Di Mise A, et al. AQP2 abundance is regulated by the E3-ligase CHIP via HSP70. *Cell Physiol Biochem*. 2017;44(2):515-531.
52. Gürtler A, Kunz N, Gomolka M, et al. Stain-free technology as a normalization tool in Western blot analysis. *Anal Biochem*. 2013;433(2):105-111.
53. Théry C, Amigorena S, Raposo G, Clayton A. Isolation and characterization of exosomes from cell culture supernatants and biological fluids. *Curr Protoc Cell Biol*. 2006;Chapter 3:Unit 3.22.
54. Tlemsani C, Pongor L, Elloumi F, et al. SCLC-CellMiner: a resource for small cell lung cancer cell line genomics and pharmacology based on genomic signatures. *Cell Rep*. 2020;33(3):108296.
55. Ho-Xuan H, GlaÅar P, Latini C, et al. Comprehensive analysis of translation from overexpressed circular RNAs reveals pervasive translation from linear transcripts. *Nucleic Acids Res*. 2020;48(18):10368-10382.
56. Hansen TB. Characterization of circular RNA concatemers. *Methods Mol Biol*. 2018;1724:143-157.
57. Ke N, Wang X, Xu X, Abassi YA. The xCELLigence system for real-time and label-free monitoring of cell viability. *Methods Mol Biol*. 2011;740:33-43.
58. Lu H, Xie X, Chen Q, et al. Clinical significance of circPVT1 in patients with non-small cell lung cancer who received cisplatin combined with gemcitabine chemotherapy. *Tumori*. 2021;107(3):204-208.
59. Shi J, Lv X, Zeng L, et al. CircPVT1 promotes proliferation of lung squamous cell carcinoma by binding to miR-30d/e. *J Exp Clin Cancer Res*. 2021;40(1):193.
60. Zheng F, Xu R. CircPVT1 contributes to chemotherapy resistance of lung adenocarcinoma through miR-145-5p/ABCC1 axis. *Biomed Pharmacother*. 2020;124:109828.
61. Danac JMC, Garcia RL. CircPVT1 attenuates negative regulation of NRAS by let-7 and drives cancer cells towards oncogenicity. *Sci Rep*. 2021;11(1):9021.
62. Huang M, Li T, Wang Q, et al. Silencing circPVT1 enhances radiosensitivity in non-small cell lung cancer by sponging microRNA-1208. *Cancer Biomark*. 2021;31(3):263-279.
63. Chen J, Li Y, Zheng Q, et al. Circular RNA profile identifies circPVT1 as a proliferative factor and prognostic marker in gastric cancer. *Cancer Lett*. 2017;388:208-219.
64. Verduci L, Ferraiuolo M, Sacconi A, et al. The oncogenic role of circPVT1 in head and neck squamous cell carcinoma is mediated through the mutant p53/YAP/TEAD transcription- competent complex. *Genome Biol*. 2017;18(1):237.
65. Hu J, Han Q, Gu Y, et al. Circular RNA PVT1 expression and its roles in acute lymphoblastic leukemia. *Epigenomics*. 2018;10(6):723-732.
66. Umemori M, Kurata M, Yamamoto A, et al. The expression of MYC is strongly dependent on the circular PVT1 expression in pure Gleason pattern 4 of prostatic cancer. *Med Mol Morphol*. 2020;53(3):156-167.
67. Palcau AC, Canu V, Donzelli S, Strano S, Pulito C, Blandino G. CircPVT1: a pivotal circular node intersecting Long non-coding-PVT1 and c-MYC oncogenic signals. *Mol Cancer*. 2022;21(1):33.
68. Panda AC, Grammatikakis I, Kim KM, et al. Identification of senescence-associated circular RNAs (SAC-RNAs) reveals senescence suppressor CircPVT1. *Nucleic Acids Res*. 2017;45(7):4021-4035.
69. Wang J, Huang K, Shi L, Zhang Q, Zhang S. CircPVT1 promoted the progression of breast cancer by regulating MiR-29a-3p-mediated AGR2-HIF-1α pathway. *Cancer Manag Res*. 2020;12:11477-11490.
70. He X, Su W, Zhou Y, Ge X, Zhou J, Ou C. CircPVT1: a bridge linking hippo pathway and human cancers. *Ann Transl Med*. 2018;6(S2):S91.
71. Wu Q, Guo J, Liu Y, et al. YAP drives fate conversion and chemoresistance of small cell lung cancer. *Sci Adv*. 2021;7(40):eabg1850.
72. Ghetti M, Vannini I, Storlazzi CT, Martinelli G, Simonetti G. Linear and circular PVT1 in hematological malignancies and immune response: two faces of the same coin. *Mol Cancer*. 2020;19(1):69.
73. Ghafouri-Fard S, Khoshbakht T, Taheri M, Jamali E. A concise review on the role of CircPVT1 in tumorigenesis, drug sensitivity, and cancer prognosis. *Front Oncol*. 2021;11:11.
74. Zheng X, Chen L, Zhou Y, et al. A novel protein encoded by a circular RNA circPPP1R12A promotes tumor pathogenesis and metastasis of colon cancer via hippo-YAP signaling. *Mol Cancer*. 2019;18(1):47.
75. Visci G, Tolomeo D, Agostini A, Traversa D, Macchia G, Storlazzi CT. CircRNAs and fusion-circRNAs in cancer: new players in an old game. *Cell Signal*. 2020;75:75.
76. Yao W, Guo P, Mu Q, Wang Y. Exosome-derived circ-PVT1 contributes to cisplatin resistance by regulating autophagy, invasion, and apoptosis via miR-30a-5p/YAP1 Axis in gastric cancer cells. *Cancer Biother Radiopharm*. 2021;36(4):347-359.
77. Sun C, Wang P, Dong W, Liu H, Sun J, Zhao L. LncRNA PVT1 promotes exosome secretion through YKT6, RAB7, and VAMP3 in pancreatic cancer. *Aging (Albany NY)*. 2020;12(11):10427-10440.

78. Rudin CM, Durinck S, Stawiski EW, et al. Comprehensive genomic analysis identifies SOX2 as a frequently amplified gene in small-cell lung cancer. *Nat Genet*. 2012;44(10):1111-1116.
79. Campbell PJ, Stephens PJ, Pleasance ED, et al. Identification of somatically acquired rearrangements in cancer using genome-wide massively parallel paired-end sequencing. *Nat Genet*. 2008;40(6):722-729.
80. Northcott PA, Shih DJH, Peacock J, et al. Subgroup-specific structural variation across 1,000 medulloblastoma genomes. *Nature*. 2012;488(7409):49-56.
81. Johansson B, Mertens F, Schyman T, Björk J, Mandahl N, Mitelman F. Most gene fusions in cancer are stochastic events. *Genes Chromosomes Cancer*. 2019;58(9):607-611.
82. Kalyana-Sundaram S, Shankar S, DeRoo S, et al. Gene fusions associated with recurrent amplicons represent a class of passenger aberrations in breast cancer. *Neoplasia*. 2012;14(8):702-708.
83. Aguado C, Giménez-Capitán A, Karachaliou N, et al. Fusion gene and splice variant analyses in liquid biopsies of lung cancer patients. *Transl Lung Cancer Res*. 2016;5(5):525-531.
84. Nilsson RJA, Karachaliou N, Berenguer J, et al. Rearranged EML4-ALK fusion transcripts sequester in circulating blood platelets and enable blood-based crizotinib response monitoring in non-small-cell lung cancer. *Oncotarget*. 2016;7(1):1066-1075.

SUPPORTING INFORMATION

Additional supporting information can be found online in the Supporting Information section at the end of this article.

How to cite this article: Tolomeo D, Traversa D, Venuto S, et al. circPVT1 and *PVT1/AKT3* show a role in cell proliferation, apoptosis, and tumor subtype-definition in small cell lung cancer. *Genes Chromosomes Cancer*. 2023;1-15. doi:10.1002/gcc.23121